Synchrotron measurements of local microstructure and residual strains in ductile cast iron

Zhang, Yubin; Andriollo, Tito; Fæster, Søren; Liu, W.; Sturlason, A.; Barabash, R.

Published in:
I O P Conference Series: Materials Science and Engineering

Link to article, DOI:
10.1088/1757-899X/219/1/012054

Publication date:
2017

Document Version
Publisher's PDF, also known as Version of record

IOP Conf. Series: Materials Science and Engineering **219** (2017) 012054 doi:10.1088/1757-899X/219/1/012054

Synchrotron measurements of local microstructure and residual strains in ductile cast iron

Y B Zhang [1], T Andriollo [2], S Fæster [1], W Liu [3], A Sturlason [4], R Barabash [5]

[1] Section for Materials Science and Advanced Characterization, Department of Wind Energy, Technical University of Denmark, Risø Campus, Roskilde 4000, Denmark
[2] Department of Mechanical Engineering, Technical University of Denmark, DK-2800 Kgs. Lyngby, Denmark
[3] Advanced Photon Source, Argonne National Laboratory, Argonne, IL, 60439-4800, USA
[4] Vestas Wind Systems A/S, 8200 Aarhus N, Denmark
[5] Materials Science & Technology Division, Oak Ridge National Laboratory, P.O. Box 2008, Oak Ridge, TN, 37831-6118, USA

E-mail: yubz@dtu.dk

Abstract. The local microstructure and distribution of thermally induced residual strains in ferrite matrix grains around an individual spherical graphite nodule in ductile cast iron (DCI) were measured using a synchrotron X-ray micro-diffraction technique. It is found that the matrix grains are deformed, containing dislocations and dislocation boundaries. Each of the residual strain components in the matrix grains exhibits a complex pattern along the circumferential direction of the nodule. Along the radial direction of the nodule, strain gradients from the interface to the grain interior are seen for some strain components, but only in some matrix grains. The observed residual strain patterns have been analysed by finite element modelling, and a comparison between the simulation and experiments is given. The present study of local residual stress by both experimental characterization and simulation provide much needed information for understanding the mechanical properties of DCI, and represent an important contribution for the microstructural design of new DCI materials.

1. Introduction

The mechanical properties of cast iron depend strongly on the microscopic morphology and distribution of the graphite particles present in the iron matrix. It is well known that spherical graphite nodules in ductile cast iron (DCI) result in better impact and fatigue resistance than graphite flakes in grey iron. Even within the DCI family, the mechanical properties are related directly to the nodularity of the graphite particles [1]. It is suggested that whereas sharp graphite flakes create stress concentration points within the metal matrix, rounded nodules reduce stress concentration and inhibit the creation of cracks [2], thereby enhancing the mechanical properties. To understand this effect and to design new DCI with improved fracture toughness and fatigue life, it is important to obtain information about the local stress in the matrix grains around individual graphite nodules.

Recently, the thermal residual strain/stress in a metal mold DCI sample has been measured using a novel synchrotron X-ray technique. It has been found that a compressive residual elastic stress with a maximum of ~180 MPa is present near the graphite nodules, extending into the matrix to a distance of

about 20 μm, where the elastic stress is near zero [3]. However, only one strain/stress component in one matrix grain around each nodule is reported in [3].

Following this previous research, the local strain tensors for several matrix grains around one graphite nodule in DCI are studied using synchrotron X-ray micro-diffraction. DCI with ferrite matrix and used broadly in modern industry was chosen for the study. The aim is to quantify the pattern of the local residual strain/stress in different matrix grains around a selected graphite nodule, and to use a finite element modelling [4] to predict the residual stresses in the matrix grains.

2. Experimental

A DCI sample cast in a metal mold was chosen for the study. The sample consists of almost spherical graphite nodules and a metal matrix with a relatively homogeneous structure, being mainly ferrite with a small fraction of pearlite (~5%). The graphite nodules, with a volume fraction of 11.5% and an average size of ~30 μm, are distributed relatively uniformly in the matrix. The ferrite matrix has an average grain size of ~30 μm. More information about the sample can be found in [3].

The synchrotron experiments were performed at beamline 34-ID-E at the Advanced Photon Source, Argonne National Laboratory using the white beam Laue micro-diffraction technique [5]. A focused microbeam with Lorentzian profile and a full-width half maximum of ~0.5 μm was used. The X-ray energies were in the range 7-30 keV. A Pt-wire of 100 μm diameter was used as a differential aperture to resolve the white beam Laue diffraction pattern from individual volume elements at different depths. The depth-resolved Laue patterns were then indexed for determining the crystallographic orientations and the deviatoric elastic strain tensor of the diffracting volume elements. This analysis was conducted using the LaueGo software package available at APS beamline 34-ID-E [6].

A graphite nodule with a size (equivalent sphere diameter) of ~50 μm was chosen, based on a tomographic characterization using a Zeiss Xradia 520 Versa μ-CT system carried out in the home laboratory prior to the synchrotron measurements. The detailed scanning position of the synchrotron X-rays relative to the selected nodule is sketched in figure 1.

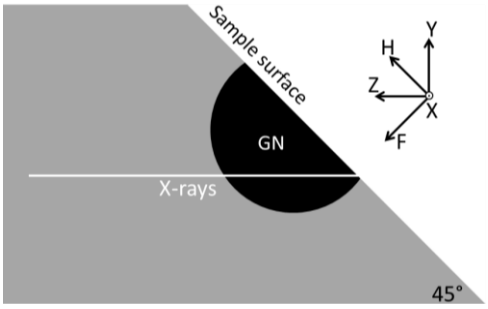

Figure 1. Sketch showing a side view of the X-ray scanning position relative to the selected graphite nodule (GN, shown in black). The white line represents the projection of the mapping plane illuminated by the incoming X-rays, which are along the Z direction. The laboratory coordinate system (X, Y, Z) and sample coordinate system (X, H, F) are defined.

3. Results and discussion

3.1. Microstructure

The microstructure in a slice (i.e. a 2D section) cutting through the selected nodule (GN) is shown in figure 2. In figure 2a, dislocation boundaries with misorientation angle higher than 0.1° are shown together with the crystallographic orientations of the matrix grains. It is found that some of the matrix grains are plastically deformed as they contain dislocation boundaries with misorientation angles up to 1°.

The number of indexed spots in the depth-resolved pattern for each volume element is shown in figure 2b. There is nearly no diffraction signal from the graphite nodule, appearing as “black holes”. In the matrix deep bulk volumes appear darker due both to X-ray absorption and plastic deformation. The non-indexed volume in the deep region may be pearlite. The volumes close to sample surface also appear dark. This is an artifact arising from reconstruction of the depth-resolved diffraction images, which creates a positional uncertainty of 2-3 μm at the real sample surface.

Figure 3a is a plot of misorientation angle to the first point measured along each of the 5 lines marked in figure 2a. The angle increases with increasing distance from the interface. The angle increase is almost monotonic, reflecting a strain gradient formed during cooling due to the different thermal contraction of the nodule and matrix. The strain gradient is a result of the strain accommodation process, leading to the formation of geometrically necessary dislocations (GNDs) [7]. The density of these dislocations can be estimated based on the misorientation angle and distance using the following equation [8]:

$$\rho = K/D_c \cdot \theta_c/b, \quad (1)$$

where K is a number typically equal to 3, D_c is the average spacing between dislocation boundaries (taken here as the distance between neighboring measurement points), θ_c is the misorientation angle between two neighboring points, and b is the Burgers vector.

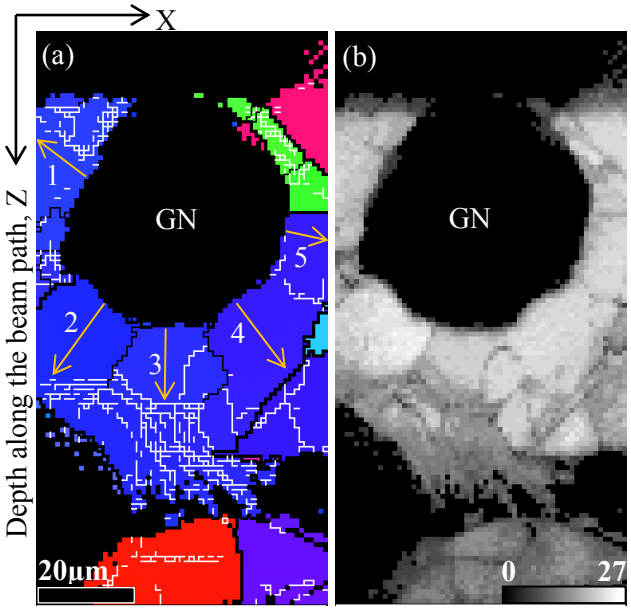

Figure 2. Microstructures of the DCI around the selected nodule GN characterized using white beam micro-diffraction. (a) is colored based on the crystallographic orientations of the matrix grains, while (b) is based on the number of indexed spots from the depth-resolved Laue diffraction images (see the inserted scale bar). In (a), dislocation boundaries with misorientation angles in the range of 0.1 – 1°, 1 – 3°, and > 3° are shown in thin white, thin black and thick black lines, respectively. The colors of the matrix grains correspond to the crystallographic orientation along the sample normal direction in the sample coordinate system (F direction in the XHF system in figure 1). Five numbered arrows mark places and directions of the misorientation analysis and quantification of dislocation density shown in figure 3.

The GND density as a function of distance from nodule/matrix interface along the 5 lines is shown in figure 3b. Despite large variations in the plot, the general tendency is that the GND density decreases within the first 5-7 μm from the interface. The increase of GND density at distances of 10-20 μm from the interface may be related to the influence of other nodules, damage during surface polishing and/or pearlite structures. The average accommodation strain within the first 5-7 μm from the interface corresponds to a dislocation density of GNDs of ~4×10^{12} m^{-2}.

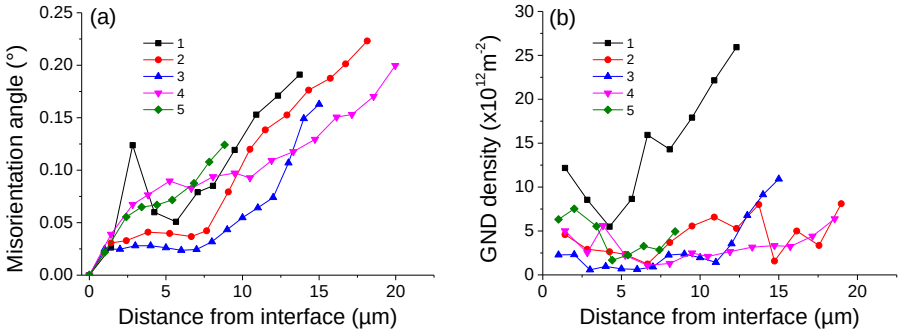

Figure 3. (a) Misorientation angles to the first point and (b) GND density estimated based on the misorientation between neighboring points along the 5 lines marked in figure 2.

3.2. Residual elastic strains

The deviatoric strain components, which represent the shape change of the crystal lattice, were determined based on the indexed depth-resolved Laue diffraction patterns. The resulting strain component maps for the matrix grains around nodule GN are shown in figure 4. The strains were determined in the sample coordinate system (i.e. XHF system in figure 1). As discussed in Refs. [9], dislocation boundaries in the matrix grains result in spot streaking in the Laue diffraction patterns and in turn exaggerate severely the deviatoric strains. Therefore, in the present study, only parts of a few grains (see figure 4) are included in the strain calculation. These parts of the grains have internal misorientation angle < 0.05°, implying that the effect of stored dislocations on spot streaking is limited, and the calculated strains are therefore trustworthy [3].

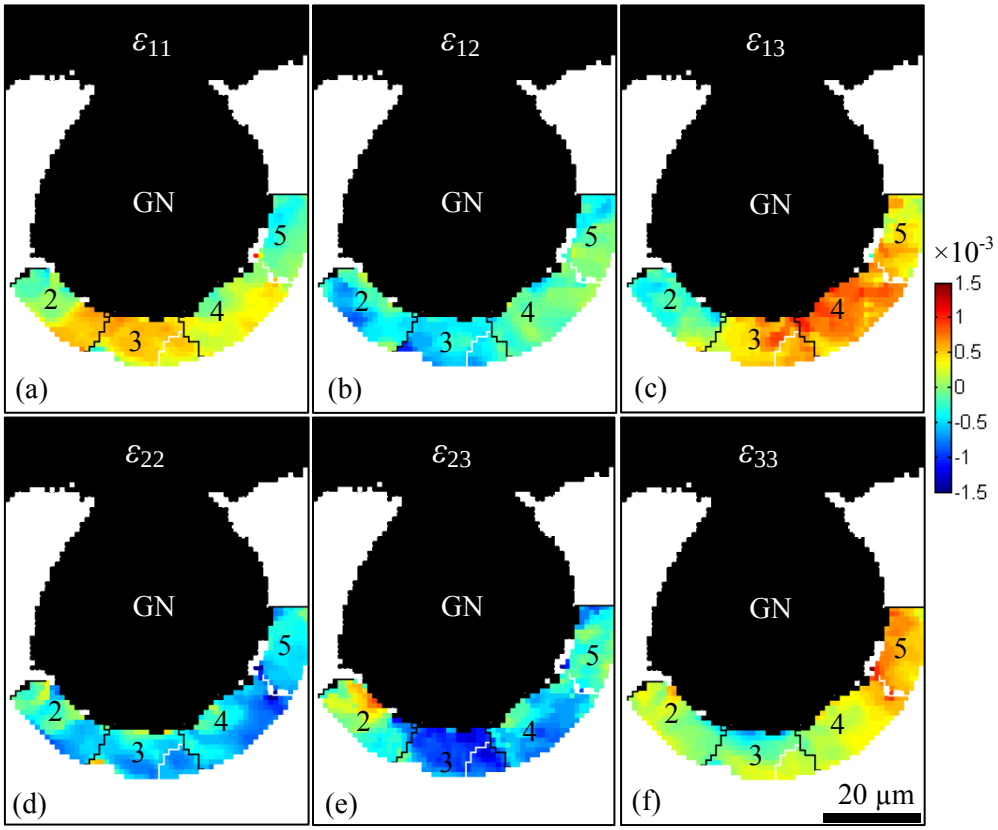

Figure 4. Strain maps colored according to the deviatoric strain components for the grains around nodule GN. Numbers are used to identify individual grains.

The strain patterns for the different strain components are quite different. When inspecting grains circumferentially around the nodule, the ε_{11} strains change gradually from mainly tensile in the bottom grain 3 to mainly compressive in grain 5. The opposite trend is seen for ε_{33}. Mainly compressive ε_{22} strains are seen for all 4 grains. For the shear strain components, the sense of ε_{13} changes from grain 2 to grains 3-5. The opposite trend is seen for ε_{23}. The majority of the ε_{12} strain has negative value, while the ε_{12} strain in grain 4 and 5 are close to zero.

Along the nodule radial directions, the strain pattern are rather complex. Strain gradients from the interface to the grain interior are seen for some strain components within some parts of the grains. For example, the magnitude of ε_{11} and ε_{33} in grains 3 and 5 decreases, while the magnitude of the compressive ε_{22} strain increases in grain 3 and in parts of grains 2, 4 and 5. In grain 4, the strain gradients for most of the strain components are less pronounced.

3.3. Finite element modelling

To understand the complex pattern of the residual strains seen in figure 4, a 3D finite element model of residual elastic strain, developed and presented in a previous publication [5], is used to calculate the residual stress/strain distribution. In this model, a graphite volume fraction of 11.5 % is used. Detailed parameters for the model can be found elsewhere [3,5].

The predicted stress maps on an X-Z section equivalent to that marked by white line in figure 1 are shown in figure 5. The predicted stress patterns are quite different for different stress components. However, symmetrical distributions with respect to the vertical Z axis or horizontal X axis or both axes can be seen for all the stress components. Due to the lack of experimental data, this symmetry cannot be examined for the experimental results.

By comparing the simulated stress pattern with the experimental pattern, some agreements are found. For example, for the ε_{11} strain component, changes from tensile at the bottom of the nodule gradually to compressive at the right side of the nodule along the nodule circumferential direction are seen both in the experimental and simulated strain pattern. Similar agreement is found for the ε_{33} strain component. For the ε_{12} component, negative and close to zero strains is seen both for the grains 4 and 5 in the experimental data and for the simulated results at the same locations. Similarly, negative ε_{23} strains for grains 3 and 4 agree with the predicted strains. However, the predicted ε_{22} strains, mainly tensile at the lower half of the nodule, are completely different from the experimental results. Similar disagreement is observed for ε_{13} component.

If the strain gradients along the radial direction are considered, the model predicts well-defined gradients for all strain components. Compared to the experimental strain gradients for ε_{11} and ε_{33} components, the model captures the gradient direction correctly. In spite of a different strain direction between the simulated and experimental results for ε_{22} component, the gradient direction is the same.

There could be several reasons for the disagreements between the simulated and experimental results. First, in the model the metal matrix is assumed to be elastically isotropic, while multiple grains with different crystallographic orientations (see figure 2a) reveal that the matrix is elastically anisotropic. Additionally, this orientation difference leads to different deformation behavior between grains [10]. Both factors can lead to local strain variations from grain to grain. More importantly, experimentally the plastic deformation is not homogeneous even within individual grains, leading to local orientation variations (see figures 2a and 3). As plastic deformation can relax the residual elastic strain/stress, the inhomogeneous plastic deformation therefore is expected to lead to inhomogeneous strain/stress distribution, which can even change the local strain gradients, along both the radial and circumferential directions. Secondly, an ideal spherical nodule is used in the model, while in reality the nodule is not perfectly spherical, which can lead again to local strain variations from location to location along the circumferential direction of the nodule. Thirdly, experimentally the nodule is exposed to free sample surface, while in the model the nodule is fully embedded in the bulk. As shown in the previous study [3], free surface can lead to reduced magnitude of ε_{33} strain for the grains at the bottom part of the nodule. To fully address how the free surface combined with a non-spherical shape

of the nodule affects the strain changes for other strain components, additional simulation work is underway.

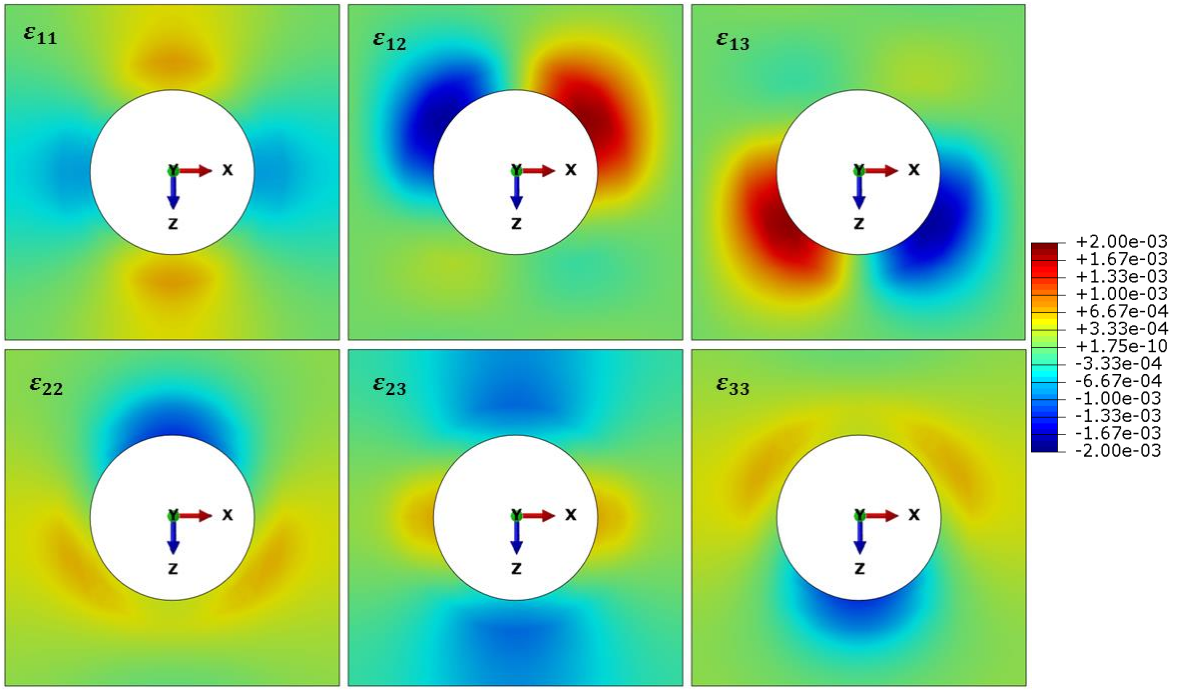

Figure 5. Strain maps colored according to the predicted strain components.

Irrespective of these reasons, a completely different strain direction for the ε_{22} and ε_{13} components between the experimental and simulated results cannot be understood. This suggest that the thermal residual stresses developed due to the difference in thermal expansion coefficients between graphite nodule and metal matrix may not be fully described by a simple thermal contraction process as used in the present model and other models based on Eshelby's equivalent inclusion method [11]. Further studies are required to clarify this aspect.

4. Conclusions

The synchrotron X-ray micro-diffraction method has been used in the present study to characterize the local microstructure and residual strain pattern in matrix grains around a graphite nodule in a ductile cast iron sample. To understand the experimentally measured strain pattern, a finite element model has been used to calculate the residual stress/strain distribution. The main findings are:

i) During cooling of DCI, differences in thermal contraction lead to deformation of the iron matrix both elastically and plastically. Within a distance of 5-7 µm from the surface of a nodule strain gradients are revealed corresponding to storage of geometrically necessary dislocations with an estimated density of ~4×10^{12} m^{-2}.

ii) Complex strain patterns are seen for all strain components of the matrix grains around the nodule. Strain gradients are seen along both the circumferential and radial directions for some grains and for some strain components.

iii) Finite element modelling considering simple thermal contraction processes captures some of the experimentally observed strain gradients along the circumferential and radial directions. However, disagreement for the ε_{22} and ε_{13} components between the predicted and experimental results suggests the mechanism for the development of thermal residual stress may be more complex than heretofore assumed.

Acknowledgments
Part of this work has been supported by the Strategic Research Center ‘‘REWIND -Knowledge based engineering for improved reliability of critical wind turbine components,’’ Danish Research Council for Strategic Research, grant no. 10-093966. Use of the Advanced Photon Source was supported by the U. S. Department of Energy, Office of Science, Office of Basic Energy Sciences, under Contract No. DE-AC02-06CH11357.

References
[1] Labrecque C and Gagne M 1998 *Can Metall Q*. **37** 343-378
[2] *Ductile iron data*.:http://www.ductile.org/ductile-iron-data-2/
[3] Zhang Y B, Andriollo T, Fæster S, Liu W, Hattel J and Barabash R I 2016 *Acta Mater*. **121** 173-180
[4] Andriollo T, Thorborg J, Tiedje N and Hattel J 2016 *Model Simulations Mater Sci Eng*. **24** 055012
[5] Larson B, Yang W, Ice G, Budai J and Tischler J 2002 *Nature* **415** 887-890
[6] Tischler J Z 2014 *Strain and Dislocation Gradients from Diffraction Ch. 10* Eds. Barabash R and Ice G E (London: Imperial College Press)
[7] Barabash R I, Ice G E and Pang J W L 2005 *Mater Sci Eng A*. **400-401** 125-131
[8] Hansen N 1994 *15th Risø Int. Symp. on Materials Science* (Roskilde: Risø) p 325-334
[9] Larson B C and Levine L E 2013 *J Appl Crystallogr*. **46** 153-164
[10] Huang X and Winther G 2007 *Philos Mag*. **87** 5189-5214
[11] Eshelby J D 1957 *Proc R Soc A Math Phys Eng Sci*. **241** 376-396